Journal of Materials Chemistry B

Accepted Manuscript

ROYAL SOCIETY OF CHEMISTRY

www.rsc.org/materialsB

Theranostic CuS Nanoparticles Targeting Folate Receptors for PET Image-Guided Photothermal Therapy

Min Zhou[a,b,#], Shaoli Song[a, c,#], Jun Zhao[a], Mei Tian[b], Chun Li[a,*]

[a]Department of Cancer Systems Imaging, The University of Texas MD Anderson Cancer Center, Houston, Texas 77054, United State.

[b]The Second Hospital of Zhejiang University, Hangzhou, Zhejiang, China

[c]Department of Nuclear Medicine, Renji Hospital, Shanghai Jiaotong University School of Medicine, Shanghai 200127, P. R. China

***Corresponding Author:**

Chun Li, Department of Cancer Systems Imaging – Unit 1907, 1881 East Road, The University of Texas MD Anderson Cancer Center, Houston, Texas 77054; Phone: (713) 792-5182; Fax: (713) 794-5456; E-mail: cli@mdanderson.org.

[#]These authors contributed equally to this work

Abstract:

Copper sulfide nanoparticles (CuS NPs) have been reported as a single-compartment theranostic nanosystem to visualize and treat tumors simultaneously. However, few studies have investigated the *in vivo* tumor-targeted delivery of this class of nanoparticles. In this study, we introduced a tumor-specific targeting ligand, folic acid (FA), onto the surface of CuS NPs as a model system to demonstrate the feasibility of actively targeted CuS NPs for positron emission tomography (PET) imaging and PET image-guided photothermal therapy (PTT). A one-pot synthetic method was used for introducing FA to CuS NPs to yield FA-CuS NPs. Biodistribution studies in mice bearing folate receptor-expressing KB tumor showed significantly higher tumor uptake of FA-CuS NPs than non-targeted polyethylene glycol (PEG)-coated PEG-CuS NPs after intravenous injection. Moreover, tumor uptake of FA-CuS NPs could be effectively blocked by free FA. Biodistribution and clearance of ^{64}Cu-labeled FA-CuS NPs (FA-[^{64}Cu]CuS NPs) could be readily visualized by microPET (μPET), which confirmed a significantly higher level of tumor uptake of FA-[^{64}Cu]CuS NPs than non-targeted PEG-[^{64}Cu]CuS NPs. μPET image-guided PTT with FA-CuS NPs mediated substantially greater tumor damage compared with PTT mediated by PEG-CuS NPs. Thus, FA-CuS NPs is a promising candidate for PTT of folate receptor-positive tumors.

Keywords: *folate targeting, theranostic, PET/CT imaging, photothermal therapy, CuS nanoparticles*

1. Introduction

Nanoparticle (NP)-based photothermal therapy (PTT) has been proposed as a minimally invasive intervention to complement surgical option [1-4]. The NPs used for PTT possess strong near-infrared (NIR) absorption (700-1100 nm). They convert absorbed photo-energy to thermal energy locally, resulting in selective ablation of solid tumors. Most photothermal-converting NPs are delivered to tumors owing to enhanced permeability and retention [EPR] effect [5]. Active targeting that introduces receptor ligands on gold-based nanoparticle's surfaces, such as small-molecular-weight peptides on hollow gold nanospheres, has also been investigated [6, 7]. Several kinds of NPs, including gold nanostructures (nanoshells, nanocages, nanorods, and hollow nanospheres),[8-17] carbon nanotubes,[18, 19] graphene,[20, 21] palladium nanosheet,[22] and copper based nanostructures,[23-25] have been investigated as efficient photothermal converting agents for PTT of cancer.Recent studies on copper sulfide (CuS) NPs have demonstrated advantages of this class of photothermal conversion agents, including simplicity of synthesis, low cost of production, high photothermal conversion efficiency, relatively small size (hydrodynamic diameter [HD] ~10-30 nm), and ability to perform repetitive treatments without changing optical properties.[26-31] Our previous studies have shown that polyethylene glycol (PEG)-coated CuS NPs (PEG-CuS NPs), delivered through a nonspecific EPR effect, could mediate effective tumor cell destruction *in vitro* and *in vivo*.[29] However, it is necessary to further enhance the delivery efficiency of CuS NPs to tumors to increase the therapeutic effect and reduce their potential toxicity. To date, few studies have investigated tumor-targeted delivery of CuS-based nanoparticles.

As a targeting ligand, Folic acid (FA) has been extensively investigated for the homing of nanoparticles to folate receptors (FRs).[14, 32-39] As a potential targeting agent, FA has much lower molecular weight (441 Da) compared to peptides and antibodies. FRs are highly expressed in

ovarian, breast, lung, and head & neck cancers. Normal tissues, on the other hand, lack FR expression. Thus, FA is a promising tumor-targeting ligand.

Here, we introduced FA onto the surface of CuS NPs as a model system to demonstrate the feasibility of actively targeted CuS NPs for positron emission tomography (PET) imaging and PET image-guided PTT. We found that FA-[^{64}Cu]CuS NPs could selectively home to FR-overexpressing human nasopharyngeal carcinoma KB tumors and that PTT mediated by FA-CuS NPs significantly enhanced antitumor efficacy at low NIR laser power densities. To the best of our knowledge, this is the first report to demonstrate active tumor targeting of CuS-based NPs.

2. Materials and methods

2.1 Materials

FA, methoxy-PEG-thiol (PEG-SH; 5000 Da), sodium sulfide (Na_2S), Cy5.5 *N*-hydroxysuccinimide (NHS) ester, copper chloride ($CuCl_2$), 4′, 6-diamidino-2-phenylindole, dimethyl formamide, and ethylenediaminetetraacetic acid were supplied by Sigma-Aldrich (St. Louis, MO). $^{64}CuCl_2$ was obtained from the University of Wisconsin–Madison or The University of Texas MD Anderson Cancer Center Cyclotron Research Facility. Isoflurane was purchased from Baxter (Deerfield, IL). Human nasopharyngeal tumor KB cells were supplied from ATCC (Manassas, VA). Ethidium homodimer I (EthD-1) and calcein AM and dyes were supplied by Invitrogen (Grand Island, NY).

2.2 Synthesis of FA-CuS NPs and PEG-CuS NPs

FA-CuS NPs were synthesized as follow: 100 μL of an aqueous solution of Na_2S (1 M) was added to $CuCl_2$ (100 mL, 1 mM) aqueous solution containing 0.16 mg FA under magnetic

stirring. The turbid yellow FA-$CuCl_2$ mixture turned clear yellow rapidly on mixing and gradually changed to a greenish color. Five minutes later, the solution was heated to 90°C. When the color of the solution changed to dark-green, the FA-CuS NPs were obtained following the solution was cooled on ice. FA-CuS NPs were purified by a PD-10 column (GE Healthcare Life Science, Pittsburgh, PA). PEG-CuS NPs were prepared following our previous report.[29]

2.3 Tagging FA-CuS NPs with Cy5.5

Briefly, Cy5.5 NHS ester (0.1 mg) was dissolved in dimethyl formamide (100 µL) and added to a 10-mL FA-CuS NPs solution (100 µg/mL, pH = 12). The solution was then vortexed and shaked overnight. The crude product was purified using a PD-10 column to yield Cy5.5-coated FA-CuS NPs.

2.4 Characterization of FA-CuS NPs

The NPs size was measured by a JEM 2010 transmission electron microscope (JEOL, Japan). The optical properties of the NPs were recorded by an UV−vis spectrometer (DU-800, Beckman Coulter, Brea, CA). Dynamic light-scattering and zeta potential (Brookhaven 90Plus, Holtsville, NY) was used to determine hydrodynamic size and surface charge of the CuS NPs. The molecular structures of the FA-CuS NPs were analyzed by a Bruker Avance 600 spectrometer (proton nuclear magnetic resonance spectroscopy (^{1}H-NMR, Billerica, MA).

In order to calculate the number of FA molecules associated with CuS NPs, a standard absorbance vs. concentration curve was generated from solutions of free FA in water. Ammonia was added to aqueous solution of FA-CuS NPs to dissolve CuS NPs and release free FA. The resulting solution was recorded by UV-vis spectroscopy. FA concentration was estimated from the FA standard curve, which was estimated to be 2 µg/mL in a 2[OD] FA-CuS NPs solution (or ~2.73×10^{15} molecules/mL). The number of CuS NPs was estimated on the basis of spherical

NPs with a density of 4.6 g/cm^3 and average diameter of 21 nm. For a 2[OD] FA-CuS NP solution (~0.1 mg/mL), the particle concentration was estimated to be 4.3 x 10^{12} particles/mL. Thus, each FA-CuS nanoparticle contained about 635 FA molecules.

2.5 Photothermal effect of the NP in aqueous solution

A continuous-wave 808-nm laser (15PLUS Laser, Diomed, Andover, MA) was used for the measurement of temperature change. The optical fiber was supplied by BioTex Inc (Houston, TX). The NIR light (808-nm, 3 W/cm^2) was passed through a quartz cuvette containing either pure water (control) or FA-CuS NPs solution (100 μg/mL, 400 μL). The temperature was measured by a thermocouple over a period of 10 min.

2.6 Stability of FA-CuS NPs

Solutions of FA-CuS NPs in water, PBS, and FBS (10% in PBS) were stored at 37°C for 7 days. Aliquots were taken at day 1 and day 7 for UV-Vis spectrum and dynamic light scattering measurement. No precipitation was observed by visual inspection.

2.7 Cytotoxicity.

HEK-293 cells were incubated with different concentration of the FA-CuS NPs (suspended in normal water and diluted in DMEM, 100 μL per well, five wells per concentration). 72 h later, the cells were washed by PBS. Then MTS in phenol free media solution was used for the cell viability test. 4 h later, absorbance at 490 nm of the samples were measured by a BioTek Instrument microplate reader. Data was reported as mean ± standard deviations.

2.8 In vitro cellular uptake of FA-CuS NPs

KB cells were incubated with 1 mL of folate-free RPMI-1640 culture medium containing Cy5.5-coated FA-CuS NPs. After incubation for 2 h, 4′, 6-diamidino-2-phenylindole was used for

the cell nuclei staining. The cellular fluorescence images were recorded by a Zeiss microscope (Axio Observer Z1, Jena, Germany). For the blocking experiments, KB cells were incubated with free folic acid (16 mg/L) for 0.5 h and then with FA-CuS NPs under the same conditions.

2.9 ^{64}Cu Labeling and stability

PEG-[^{64}Cu]CuS NPs were prepared as previously reported.[29] For the synthesis of FA-[^{64}Cu]CuS NPs, 1 mL of $CuCl_2$ solution (1 mM) containing FA (1.6 mg/L，3.6 μM) was mixed with $^{64}CuCl_2$ (20 μL, 37 MBq). Sodium sulfide solution (10 μL, 100 mM) was then added to the mixture. After 15 min heating at 90°C, the resulting solution was cooled on ice to yield FA-[^{64}Cu]CuS NPs. The radiolabeling efficiency and stability of the ^{64}Cu labeled NPs were tested using instant thin-layer chromatography (ITLC). The ITLC strips were developed with PBS (pH 7.4) containing 4 mM ethylenediaminetetraacetic acid (EDTA) and quantified using an ITLC imaging scanner (Bioscan IAR-2000, Washington, DC). The radiolabeled CuS NPs remained at the original spot, while free $^{64}Cu^{2+}$ ions was captured by EDTA and shifted to strip front. FA-[^{64}Cu]CuS NP solution was incubated in PBS for 48 h at 37°C for the study of labeling stability,. The solution was then analyzed by ITLC and UV-vis spectroscopy to document changes in percentage of NP-associated radioactivity and shift in the NIR absorption spectra, respectively.

2.10 Pharmacokinetics and biodistribution

All animal handling procedures were in accordance with the guidelines of the Institutional Animal Care and Use Committee of The University of Texas MD Anderson Cancer Center (Houston, TX) and were performed under a protocol approved by this committee. For pharmacokinetic analysis, each female mouse received intravenous injection of FA-[^{64}Cu]CuS NPs (1.85 MBq/mouse in 200 μL) (n = 5/group). Ten microliter of blood samples were collected from the tail vein at various time points. A Packard Cobra gamma counter (Ramsey, MN) was

used to count the radioactivity. The percentage of the injected dose per gram of blood (%ID/g) was calculated. A two-compartmental model using was used for the blood pharmacokinetic analysis.

To investigate the *in vivo* biodistribution of FA-CuS NPs, 1×10^6 KB tumor cells were inoculated subcutaneously in the left axillae of nude mice (20−25 g). When the tumors size reached 5-8 mm, the mice were randomly assigned into 3 groups (n = 5). Mice in group 1 were intravenously injected with FA-[^{64}Cu]CuS NPs (200 μL, 0.75 MBq/mouse); mice in group 2 were intravenously injected with PEG-[^{64}Cu]CuS NPs (200 μL, 0.75 MBq/mouse); and mice in group 3 were intravenously injected with an excess of free FA (200 μL, 1.6 mg/L, 3.6 μM) followed by injection of FA-[^{64}Cu]CuS NPs (200 μL, 0.75 MBq/mouse) 2 h later. 24 h after injection, mice were sacrificed by CO_2. Major organs including tumor tissues were removed, weighed, and radioactivity counted with a gamma counter. The tissue uptake of the ^{64}Cu-labeled CuS NPs was expressed as %ID/g. A biodistribution study of FA-[^{64}Cu]CuS NPs was also conducted in nude mice bearing orthotopic human HeyA8 ovarian tumors using the same procedures. For HeyA8 tumor model, tumor cells were grown in nude mice (20−25 g) by intraperitoneal injection of 1×10^6 tumor cells.

2.11 PET/CT imaging

Mice bearing KB tumors were prepared as described above. When the tumor size reached 5-8 mm in diameter, the mice (n = 3/group) were treated with an intravenous injection of FA-[^{64}Cu]CuS NPs (200 μL, 7.4 MBq/mouse), PEG-[^{64}Cu]CuS NPs (200 μL, 7.4 MBq/mouse), or intravenous injection of a large excess of free FA followed by FA-[^{64}Cu]CuS NPs (200 μL, 7.4 MBq/mouse) 2 h later. uPET/CT images were acquired by an PET/CT scanner (Siemens, Knoxville, TN) 24 h after injection. For data analysis, the region-of-interest for the tumor and muscle was defined manually, and the mean signal intensities in the region-of-interest were

recorded. Mice were killed by CO_2 overexposure after PET/CT imaging. The tumors were removed, snap-frozen, and cut into 50-μm slices. Sections were air-dried, exposed to phosphor screen, and analyzed by an autoradiography imaging system (Fujifilm FLA-5100, Cypress, CA).

2.12 In vitro Photothermal therapy of cancer cells mediated by CuS NPs

KB cells were incubated with FA-CuS NPs (100 μg/mL) or PEG-CuS NPs (100 μg/mL) in folate-free RPMI-1640 culture medium (Invitrogen, Carlsbad, CA) at 37°C. Cells with no treatment were used as a control. After 2 h, the culture medium was replaced with fresh folate-free RPMI-1640 medium without phenol red. The cells were then exposed to an 808-nm NIR laser at 1.5 W/cm^2 for 2 min. After treatment, folate-free RPMI-1640 containing 10% FBS was added and the cells incubated for an additional 24 h. The cells were washed with HBSS culture medium, and stained with EthD-1 and calcein AM according to the manufacturer's suggested protocol (Invitrogen). Cells were examined under Zeiss fluorescence microscope for visualization of dead and viable cells.

2.13 In vivo photothermal therapy of KB tumors

Nude mice bearing KB tumors were prepared as described above. When the tumors size reached 5-8 mm in diameter, the mice were assigned into three groups (n = 3/group). Mice in group 1 and group 2 were injected intravenously with FA-CuS NPs (200 μg/mL, 200 μL/mouse) and PEG-CuS NPs (200 μg/mL, 200 μL/mouse), respectively. Saline was i.v. injected to the mice in group 3. 24 h later, the tumors in mice of all groups were treated by the 808-nm NIR laser at power density of 1.5 W/cm^2 for 2 min. The temperature change of the tumors was monitored by an infrared thermal imaging camera (FLIR I7, Boston, MA) during laser treatment. 24 h after laser treatment, the mice were sacrificed and the tumors were collected for the hematoxylin & eosin staining. The damage of the tumors was examined by a fluorescence

microscope (Zeiss). The extent of tumor damage was expressed as percentage of necrosis, which was defined as: Area(necrosis zone) / Area(whole tumor)*100. Aperio Digital Pathology software (Leica Biosystems, Buffalo Grove, IL) was used for the analysis.

2.14 Statistical Analysis

Differences in pharmacokinetic characteristics, biodistribution data, and tumor damage between different study conditions and mouse groups were analyzed using the two-tailed Student's *t*-test. Differences between groups were considered statistically significant at $p < 0.05$.

3. Results and discussion

3.1 Synthesis, characterization, and stability of FA-CuS NPs

In our original report, citric acid-coated CuS NPS were synthesized from aqueous solutions of $CuCl_2$ and Na_2S containing citric acid.[29] Surface-coated citric acid molecules stabilized the resulting NPs. The structural similarity between citric acid and folic acid (both contained multiple carboxylic acid groups) prompted us to explore whether folic acid could be directly introduced to CuS NPs using a approach similar to that used in the synthesis of citric acid-coated CuS NPs (**Scheme 1a)**. Zetal potential analysis showed that FA-CuS NPs had negative charge (-27.88 mV, **Figure S1**), which provided the electrostatic repulsion for their stability. ^{1}H-NMR analysis confirmed that using this simple synthesis procedure, FA was successfully bound onto the CuS NPs' surface (**Figure S2**). Based on UV/Vis absorbance of free folic acid released from FA-CuS NPs, there were about 635 FA molecules on each CuS NP. **Figure 1a** shows a typical TEM image of the resulting FA-CuS NPs. The average size of the FA-CuS NPs was ~12 nm. The corresponding mean hydrodynamic size of FA-CuS NPs was 21 nm (**Figure 1b**). In comparison,

the mean particle size of PEG-CuS NPs increased from 11.3 nm as determined by TEM to 31 nm as determined by the light-scattering technique, reflecting the fact that the PEG coating formed a much thicker hydrophilic shell around the CuS core than did the FA coating. **Figure 1c** shows UV-vis spectrum of the FA-CuS NPs in water. A strong absorption band of the NPs was found in the NIR region. **Figure 1d** displays the temperature elevation of an aqueous solution of FA-CuS NPs as a function of exposure time to NIR light. Under NIR laser irradiation (continuous wavelength laser, 808 nm, 3 W/cm^2), the temperature of the FA-CuS NPs solution increased from 25ºC to 73ºC within 3 min and reached 84ºC after 9 min. Similar exposure time-dependent temperature elevation was also observed when the lower laser power density (1.5 W/cm^2) was used (**Figure S3**). No significant temperature change in was found for pure water under the same laser irradiation. Temperature elevation mediated by FA-CuS NPs was also concentration dependent (**Figure 1e**). FA-CuS NPs displayed excellent colloidal stability. No precipitates nor any changes in optical properties for FA-CuS NPs was found after incubation of the NPs in PBS, or PBS solution containing 10% FBS up to 7 days (**Figure 1f, Figure S4)**. Taken together, these data suggest that FA-CuS NPs are a promising candidate for efficient cancer PTT.

3.2 In vitro cytotoxicity and binding study in cancer cells

The standard MTS assay was used to evaluate the viabilities of human embryonic kidney 293 (HEK-293) cells under exposure to FA-CuS NPs. After cells were incubated with FA-CuS NPs at different concentration for 72 h, no significant cytotoxicity of FA-CuS NPs was observed at concentrations up to 400 μg/mL (**Figure 2a**).

Conjugation of Cy5.5 dye to FA-CuS NPs enabled fluorescence imaging of the cellular uptake of FA-CuS NPs. KB cells incubation with Cy5.5-labeled FA-CuS NPs for 2 h displayed higher fluorescence intensity than cells incubated with PEG-CuS NPs **(Figure 2b)**. The addition of free FA into the medium induced a significant decrease in the cell uptake of FA-CuS NPs.

This observation suggests that the FA on the surface of CuS NPs facilitated the uptake of the NPs by KB cells through FR-mediated endocytosis.

3.3 Radiolabeling, pharmacokinetics, biodistribution, and PET/CT imaging

The radioactive FA-[^{64}Cu]CuS NPs were synthesized using the same method used for the preparation of non-radioactive FA-CuS NPs, except that radioactive $^{64}CuCl_2$ together with cold $CuCl_2$ was mixed during the synthesis of CuS NPs (see **Scheme 1b**). As shown in **Figure S5**, the radiolabeling efficiency approached 99.8%, with >99% of the radioactivity associated with the FA-[^{64}Cu]CuS NPs after synthesis. The UV-vis spectrum (**Figure S6**) and hydrodynamic diameter (**Figure S7**) of FA-[^{64}Cu]CuS NPs correlated well with the non-radioactive CuS NPs, indicating that the presence of trace amount of ^{64}Cu in FA-[^{64}Cu]CuS NPs did not change the physicochemical properties of FA-CuS NPs. More than 95% of ^{64}Cu remained associated with FA-[^{64}Cu]CuS NPs after a 24-h incubation period in 10% FBS-PBS solution (**Figure S8**). These data indicated that FA-[^{64}Cu]CuS NPs have high stability and could be used for *in vivo* imaging and therapy studies.

The blood activity-time profile of FA-[^{64}Cu]CuS NPs is presented in **Figure 3,** and the corresponding pharmacokinetic profiles are shown in **Table 1**. Compared with the PEG-[^{64}Cu]CuS NPs, the FA-[^{64}Cu]CuS NPs showed different distribution characteristics *in vivo*. The mean systemic clearance of FA-[^{64}Cu]CuS NPs (2.43 mL/h) was significantly faster than that of PEG-[^{64}Cu]CuS NPs (0.48 mL/h, p = 0.0012). This may be attributed to higher accumulation of FA-[^{64}Cu]CuS NPs in organs of the mononuclear phagocytic system and accordingly faster removal from the blood of FA-[^{64}Cu]CuS NPs than of PEG-[^{64}Cu]CuS NPs. As a result, PEG-

[^{64}Cu]CuS NPs had significantly higher systemic exposure (i.e., area under the curve [AUC] = 213 %ID h/mL) than did FA-[^{64}Cu]CuS NPs (AUC = 43 %ID h/mL, $p < 0.001$). The mean volume of distribution at steady state was higher with FA-coated NPs (15.10 mL) than with PEG-coated NPs (3.79 mL, $p = 0.0015$), suggesting that FA-coated NPs had higher uptake in tissues such as the liver.

To determine the efficiency of tumor targeting with the FA-[^{64}Cu]CuS NPs, we next carried out *in vivo* biodistribution studies in tumor-bearing mice. Biodistribution data obtained 24 h after intravenous injection of FA-[^{64}Cu]CuS NPs and PEG-[^{64}Cu]CuS NPs are shown in **Figure 4**. FA-[^{64}Cu]CuS NPs accumulated at a significantly higher level in KB tumors (9.67 %ID/g) than did non-targeted PEG-[^{64}Cu]CuS NPs (6.37 %ID/g, $p = 0.01$). Furthermore, free FA (blocking group) significantly reduced the uptake of FA-[^{64}Cu]CuS NPs in KB tumors; tumor uptake of FA-[^{64}Cu]CuS NPs with FA (2.29 %ID/g) was only 23.7% that of the tumor uptake of the NPs in the absence of FA (9.67 %ID/g) $p = 0.0005$). The average tumor-to-muscle ratios for FA-[^{64}Cu]CuS NPs, PEG-[^{64}Cu]CuS NPs, and FA-[^{64}Cu]CuS NPs plus FA were 33.99, 26.41, and 8.86, respectively. In addition, we showed that FA-[^{64}Cu]CuS NPs had a relatively high uptake (8.7 %ID/g) in human HeyA8 ovarian tumors that express a moderate level of folate receptors (**Figure S9**). These results indicate that FA-CuS NPs actively target tumors expressing folate receptors.

We also performed μPET/CT imaging of KB tumor-bearing mice (**Figure 5**). Consistent with the biodistribution, μPET/CT imaging showed significant radioactivity in the liver for both FA-[^{64}Cu]CuS NPs and PEG-[^{64}Cu]CuS NPs. By 24 h after intravenous injection, accumulation of FA-CuS NPs in the tumor was clearly visualized (**Figure 5a**). Similarly, tumor uptake of the non-targeted PEG-[^{64}Cu]CuS NPs occurred, as visualized by μPET/CT, albeit to a lesser degree than the tumor uptake of targeted FA-[^{64}Cu]CuS NPs (**Figure 5b**). The uptake of FA-CuS NPs in the KB tumors was effectively blocked by an excess of free FA (**Figure 5c**). Quantitative region-

of-interest analysis showed an uptake value of 9.21 %ID/g for FA-[^{64}Cu]CuS NPs in KB tumors at 24 h post-injection, whereas the uptake of non-targeted PEG-[^{64}Cu]CuS NPs was 5.83 %ID/g ($p = 0.02$) and the uptake of FA-[^{64}Cu]CuS NPs plus free FA was 1.29 %ID/g ($p = 0.001$). Autoradiography of KB tumors also showed much higher ^{64}Cu radioactivity signals with FA-[^{64}Cu]CuS NPs than with PEG-[^{64}Cu]CuS NPs or with FA-[^{64}Cu]CuS NPs plus free FA (**Figure 5d-f**). Taken together, the pharmacokinetics, biodistribution and PET imaging data indicate that FA-[^{64}Cu]CuS NPs were delivered to the KB tumors selectively through folate receptor-mediated process.

3.4 In vitro photothermal therapy

At 24 h after laser treatment, cells pre-treated with FA-CuS NPs for 2 h were completely ablated by NIR irradiation at 1.5 W/cm^2 for 2 min. In comparison, about 60% of the cells pre-treated with PEG-CuS NPs remained viable after NIR irradiation. The addition of free FA to cells treated with FA-CuS NPs reduced the number of cells that were ablated by laser treatment (**Figure 6**). No apparent changes in cell viability were observed when cells were treated with FA-CuS NPs, PEG-CuS NPs, or blocking without NIR irradiation.

3.5 In vivo PET image-guided photothermal therapy

Since FA-[^{64}Cu]CuS NPs demonstrated higher tumor uptake than PEG-CuS NPs 24 h after intravenous injection, we chose the 24 h time point for the *in vivo* PTT treatment study. The maximum temperatures (T_{max}) in the tumors of mice who received prior injections of FA-CuS NPs, PEG-CuS NPs, and saline followed by 808-nm laser treatment at a power density of, 1.5 W/cm^2 for 2 min were 56.7°C, 42.0°C, and 35.6°C, respectively (**Figure 7**). The higher T_{max} achieved with FA-CuS NPs was attributed to their higher tumor accumulation compared with non-targeted PEG-CuS NPs. Next, we evaluated the treatment response by histological

analyses of treated tumors excised at 24 h post-laser treatment. PTT mediated by FA-CuS NPs caused more tumor damage than did PTT mediated by PEG-CuS NPs and saline. In the mice treated with FA-CuS NPs plus NIR laser, almost the entire tumor was necrotized (**Figure 8a & 8d**). Notably, this was achieved at a moderate laser power density of 1.5 W/cm^2 for a duration of only 2 min. In the mice treated with PEG-CuS NPs plus NIR laser, extensive necrosis of the tumors was also found, but with a zone of viable tumor cells remaining in the periphery of the tumor (**Figure 8b & 8e**). About 42% of the tumor tissue was necrotized in this group of mice. For the control mice treated with saline and PTT, the majority of tumor cells remained viable, with a small fraction of spontaneous necrosis observed throughout the tumor (**Figure 8c & 8f**). The percentage of necrosis in tumors treated with FA-CuS NPs plus PTT was significantly greater than that in tumors treated with PEG-CuS NPs plus PTT (p = 0.001) and saline plus PTT (p = 0.0001). These results indicate that FA-CuS NPs targeted to FA receptors mediated efficient photothermal destruction of KB tumors *in vivo*.

The *in vivo* data were supported by *in vitro* observations that cellular uptake of FA-CuS NPs in FR-expressing KB cells could be blocked by free FA (**Fig. 2**) and that FA-CuS NPs but not PEG-CuS NPs or FA-CuS NPs plus FA mediated complete ablation of KB cells in the laser irradiation zone (**Fig. 6a-6h**). Thus, FA mediated selective uptake of the CuS NPs in KB tumor cells and selective destruction of KB cells exposed to NIR laser light.

In our previous report, efficient PTT treatment of tumors in mice injected with 800 μg/mL PEG-CuS NPs (200 μL/mouse) was achieved with a higher laser power density of 12 W/cm^2 with 5 min irradiation.[29] In our current study, PTT therapy with targeted FA-CuS NPs achieved significant tumor ablation at an injection dose of 200 μL of 200 μg/mL FA-CuS NPs per mouse and a laser power density of 1.5 W/cm^2 for 2 min, effectively reducing the dose of injected NPs to 25% that of the non-targeted PEG-CuS NPs and the laser energy required with targeted NPs to 5% of what was needed with the non-targeted PEG-CuS NPs. PTT with targeted

photothermal conducting agents such as FA-CuS NPs may thus potentially translate into lower systemic toxicity and less unnecessary damage to surrounding normal tissues. Tian et al.[27] reported flower-like CuS superstructures as an efficient 980 nm laser-induced photothermal agent to ablate cancer cells. The CuS superstructures exhibited a high NIR photothermal conversion efficiency. However, the relatively large size of such particles (>500 nm) may limit their potential clinical translation.

One of the limitations of FA-CuS NPs is their relatively short half-life in blood circulation, high uptake in organs of the mononuclear phagocytic systems (i.e. liver and spleen). This led to high background signals in the PET/CT images acquired with FA-[^{64}Cu]CuS NPs. Efforts to reduce non-specific uptake of CuS NPs in general and FA-CuS NPs in specific in the liver and the spleen are currently under way. Another issue is the size of the ablation zone. The limited penetration depth of NIR light (~ 5 mm) limits the size of thermal ablation zone. Future studies will need to deploy techniques that allow deeper penetration of NIR light, such as using a pulsed laser [30] or cooling laser applicators using a water-cooled laser fiber to reduce char formation.

4. Conclusions

In this work, we show that with a simple “one-pot” synthetic process, FA could be readily coated to the surface of CuS NPs to yield highly efficient photothermal conducting agent targeted to folate receptors. Although FA-CuS NPs had a significantly shorter blood half-life than non-targeted PEG-CuS NPs, they demonstrated significantly higher tumor uptake than PEG-CuS NPs. Moreover, tumor uptake of FA-CuS NPs was largely blocked by injection of a large excess free FA. Targeted delivery of FA-CuS NPs was further confirmed by uPET/CT studies, which showed much higher tumor deposition of FA-[^{64}Cu]CuS NPs than PEG-[^{64}Cu]CuS NPs, and blockage of tumor uptake of FA-[^{64}Cu]CuS NPs by FA. Taken together, these results indicate that tumor uptake of FA-CuS NPs was mediated by FR. Successful PTT therapy

mediated by FA-CuS NPs induced almost complete tumor ablation at a remarkably low injected dose of FA-CuS NPs and low applied laser power density. Future studies will need to focus on optimizing the delivery of CuS NPs to tumor and reducing uptake in normal tissues.

Supplementary material

Details on methods used for NMR analysis, radiolabeling efficiency and stability, dynamic light scatting, and biodistribution of FA-[^{64}Cu]CuS NPs in orthotopic HeyA8.

AUTHOR INFORMATION

Corresponding Author

***Tel: 713-792-5182; Fax: 713-794-5456. E-mail: cli@mdanderson.org.

Author Contributions

[1] These authors contributed equally to this work

Notes

The authors declare no competing financial interest.

Acknowledgement

We thank Dawn Chalaire for editing this manuscript. We also acknowledge the NCI Cancer Center Support Grant CA016672, which supports MD Anderson's Small Animal Imaging Facility, NMR, and TEM Core Facilities. This work was supported in part by the John S. Dunn Research Foundation.

References

1. R. Bardhan, S. Lal, A. Joshi and N. J. Halas, *Acc. Chem. Res.*, 2011, **44**, 936-946.
2. M. P. Melancon, R. J. Stafford and C. Li, *J Controlled Release*, 2012, **164**, 177-182.
3. M. P. Melancon, M. Zhou and C. Li, *Acc. Chem. Res.*, 2011, **44**, 947-956.
4. Y. Xia, W. Li, C. M. Cobley, J. Chen, X. Xia, Q. Zhang, M. Yang, E. C. Cho and P. K. Brown, *Acc. Chem. Res.*, 2011, **44**, 914-924.
5. W. Lu, Q. Huang, K. B. Geng, X. X. Wen, M. Zhou, D. Guzatov, P. Brecht, R. Su, A. Oraevsky, L. V. Wang and C. Li, *Biomaterials*, 2010, **31**, 2617-2626.
6. W. Lu, M. P. Melancon, C. Y. Xiong, Q. Huang, A. Elliott, S. L. Song, R. Zhang, L. G. Flores, J. G. Gelovani, L. H. V. Wang, G. Ku, R. J. Stafford and C. Li, *Cancer Res.*, 2011, **71**, 6116-6121.
7. J. You, R. Zhang, C. Xiong, M. Zhong, M. Melancon, S. Gupta, A. M. Nick, A. K. Sood and C. Li, *Cancer Res.*, 2012, **72**, 4777-4786.
8. C. Loo, A. Lowery, N. J. Halas, J. West and R. Drezek, *Nano Lett.*, 2005, **5**, 709-711.
9. J. A. Schwartz, A. M. Shetty, R. E. Price, R. J. Stafford, J. C. Wang, R. K. Uthamanthil, K. Pham, R. J. McNichols, C. L. Coleman and J. D. Payne, *Cancer Res.*, 2009, **69**, 1659-1667.
10. X. H. Huang, I. H. El-Sayed, W. Qian and M. A. El-Sayed, *J. Am. Chem. Soc.*, 2006, **128**, 2115-2120.
11. X. H. Huang, P. K. Jain, I. H. El-Sayed and M. A. El-Sayed, *Laser Med. Sci.*, 2008, **23**, 217-228.
12. Y. Xia, W. Li, C. M. Cobley, J. Chen, X. Xia, Q. Zhang, M. Yang, E. C. Cho and P. K. Brown, *Acc. Chem. Res.*, 2011, **44**, 914-924.
13. J. Y. Chen, C. Glaus, R. Laforest, Q. Zhang, M. X. Yang, M. Gidding, M. J. Welch and Y. N. Xia, *Small*, 2010, **6**, 811-817.

14. W. Lu, G. Zhang, R. Zhang, L. G. Flores, 2nd, Q. Huang, J. G. Gelovani and C. Li, *Cancer Res.*, 2010, **70**, 3177-3188.

15. M. P. Melancon, W. Lu, Z. Yang, R. Zhang, Z. Cheng, A. M. Elliot, J. Stafford, T. Olson, J. Z. Zhang and C. Li, *Mol. Cancer Ther.*, 2008, **7**, 1730-1739.

16. X. Liu, N. Huang, H. Li, H. Wang, Q. Jin and J. Ji, *ACS Appl. Mater. Interfaces*, 2014, **6**, 5657-5668.

17. S. Fazal, A. Jayasree, S. Sasidharan, M. Koyakutty, S. V. Nair and D. Menon, *ACS Appl. Mater. Interfaces*, 2014, **6**, 8080-8089.

18. A. L. Antaris, J. T. Robinson, O. K. Yaghi, G. Hong, S. Diao, R. Luong and H. Dai, *ACS Nano*, 2013, **7**, 3644-3652.

19. H. K. Moon, S. H. Lee and H. C. Choi, *ACS Nano*, 2009, **3**, 3707-3713.

20. J. T. Robinson, S. M. Tabakman, Y. Y. Liang, H. L. Wang, H. S. Casalongue, D. Vinh and H. J. Dai, *J. Am. Chem. Soc.*, 2011, **133**, 6825-6831.

21. K. Yang, S. A. Zhang, G. X. Zhang, X. M. Sun, S. T. Lee and Z. A. Liu, *Nano Lett.*, 2010, **10**, 3318-3323.

22. X. Q. Huang, S. H. Tang, X. L. Mu, Y. Dai, G. X. Chen, Z. Y. Zhou, F. X. Ruan, Z. L. Yang and N. F. Zheng, *Nat Nanotechnol*, 2011, **6**, 28-32.

23. C. M. Hessel, V. P. Pattani, M. Rasch, M. G. Panthani, B. Koo, J. W. Tunnell and B. A. Korgel, *Nano Lett.*, 2011, **11**, 2560-2566.

24. L. R. Guo, D. D. Yan, D. F. Yang, Y. J. Li, X. D. Wang, O. Zalewski, B. F. Yan and W. Lu, *ACS Nano*, 2014, **8**, 5670-5681.

25. S. H. Wang, A. Riedinger, H. B. Li, C. H. Fu, H. Y. Liu, L. L. Li, T. L. Liu, L. F. Tan, M. J. Barthel, G. Pugliese, F. De Donato, M. S. D'Abbusco, X. W. Meng, L. Manna, H. Meng and T. Pellegrino, *ACS Nano*, 2015, **9**, 1788-1800.

26. Y. B. Li, W. Lu, Q. A. Huang, M. A. Huang, C. Li and W. Chen, *Nanomedicine*, 2010, **5**, 1161-1171.
27. Q. W. Tian, M. H. Tang, Y. G. Sun, R. J. Zou, Z. G. Chen, M. F. Zhu, S. P. Yang, J. L. Wang, J. H. Wang and J. Q. Hu, *Adv. Mater.*, 2011, **23**, 3542-3547.
28. S. Ramadan, L. R. Guo, Y. J. Li, B. F. Yan and W. Lu, *Small*, 2012, **8**, 3143-3150.
29. M. Zhou, R. Zhang, M. Huang, W. Lu, S. Song, M. P. Melancon, M. Tian, D. Liang and C. Li, *J. Am. Chem. Soc.*, 2010, **132**, 15351-15358.
30. M. Zhou, G. Ku, L. Pageon and C. Li, *Nanoscale*, 2014, **6**, 15228-15235.
31. B. Li, Q. Wang, R. J. Zou, X. J. Liu, K. B. Xu, W. Y. Li and J. Q. Hu, *Nanoscale*, 2014, **6**, 3274-3282.
32. J. Sudimack and R. J. Lee, *Adv. Drug Deliver. Rev.*, 2000, **41**, 147-162.
33. N. V. Nukolova, H. S. Oberoi, S. M. Cohen, A. V. Kabanov and T. K. Bronich, *Biomaterials*, 2011, **32**, 5417-5426.
34. S. Setua, D. Menon, A. Asok, S. Nair and M. Koyakutty, *Biomaterials*, 2010, **31**, 714-729.
35. V. Dixit, J. Van den Bossche, D. M. Sherman, D. H. Thompson and R. P. Andres, *Bioconjugate Chem.*, 2006, **17**, 603-609.
36. P. Chan, M. Kurisawa, J. E. Chung and Y.-Y. Yang, *Biomaterials*, 2007, **28**, 540-549.
37. J. Pan and S.-S. Feng, *Biomaterials*, 2009, **30**, 1176-1183.
38. M. B. Zheng, P. F. Zhao, Z. Y. Luo, P. Gong, C. F. Zheng, P. F. Zhang, C. X. Yue, D. Y. Gao, Y. F. Ma and L. T. Cai, *ACS Appl. Mater. Interfaces*, 2014, **6**, 6709-6716.
39. X. L. Hu, J. Tian, T. Liu, G. Y. Zhang and S. Y. Liu, *Macromolecules*, 2013, **46**, 6243-6256.

Table 1 Comparison of pharmacokinetic parameters for FA-[^{64}Cu]CuS NPs and PEG-[^{64}Cu]CuS NPs* after intravenous injection in female Swiss mice.

	$t_{1/2}\alpha$ (h)	$t_{1/2}\beta$ (h)	AUC (%ID h/mL)	Vd(ss) (mL)	Vc (mL)	CL (mL/h)	MRT (h)
FA-[^{64}Cu]CuS NPs	0.79 ± 0.21	7.78 ± 0.84	43.07 ± 10.65	15.10 ± 3.26	4.98 ± 0.45	2.43 ± 0.53	6.33 ± 1.41
PEG-[^{64}Cu]CuS NPs	0.71 ± 0.03	6.06 ± 0.03	213.70 ± 0.03	3.79 ± 0.03	2.39 ± 0.03	0.48 ± 0.03	8.05 ± 0.03

*PEG-[^{64}Cu]CuS NPs data published with permission (ref 11). Values are means ± standard deviations. Abbreviations: $t_{1/2}^{\alpha}$, blood distribution half-life; $t_{1/2}^{\beta}$, blood terminal elimination half-life; AUC, area under the blood activity-time curve; V_d(ss), volume of distribution at steady-state; V_c, volume of distribution in the central compartment; CL, total body clearance; MRT, mean residence time.

Figure Legends

Scheme 1: Schematic presentation of the synthesis of (a) FA-CuS NPs and (b) FA-[^{64}Cu]CuS NPs.

Figure 1. Characterization of FA-CuS NPs. a) TEM photograph of FA-CuS NPs, average size is ~12 nm; b) Hydrodynamic diameter distribution of FA-CuS NP samples determined by dynamic light-scattering measurement; c) Extinction spectra of 100 μg/mL) FA-CuS NPs in aqueous solution; d) Temperature change curve of FA-CuS NPs under NIR laser irradiation (808 nm, 3 W/cm^2); e) Thermal images of FA-CuS NPs with different concentration under laser irradiation for 10 min (808 nm, 3 W/cm^2); f) Stability of FA-CuS NPs, NPs were incubated in water, PBS, and PBS containing 10% FBS at 37°C for up to 7 days.

Figure 2. *In vitro* study of FA-CuS NPs. a) Viabilities of HEK-293 cells after being incubated with various concentration of FA-CuS NPs for 72 h. Error bars were based on the standard deviations (SD) of six parallel samples. b) Cellular uptake of FA-CuS and FA-CuS plus free FA. Representative fluorescence images of KB cells after incubation with FA-CuS NPs for 2 h. The red fluorescence signal is from Cy5.5-conjugated FA-CuS NPs. Cell nuclei were counterstained with 4′, 6-diamidino-2-phenylindole (DAPI; blue).

Figure 3. Activity–time profiles of FA-[^{64}Cu]CuS NPs and PEG-[^{64}Cu]CuS NPs in Swiss mice. The data are expressed as percentages of the injected dose per gram of blood (%ID/g) and are presented as mean ± SD (n = 6). PEG-[^{64}Cu]CuS NPs data published with permission (ref.11).

Figure 4. a) Biodistribution of FA-[^{64}Cu]CuS NPs, FA-[^{64}Cu]CuS NPs with blocking, and PEG-[^{64}Cu]CuS NPs in organs and tumors of nude mice at 24 h after injection. B) Comparison of nanoparticle uptake in KB tumors at 24 h post-injection. The data are expressed as

percentages of the injected dose per gram of tissue (%ID/g) and are presented as mean ± SD (n = 5). *, $p < 0.05$.

Figure 5. PET/CT imaging and autoradiography of FA-[^{64}Cu]CuS NPs and PEG-[^{64}Cu]CuS NPs. (**a-c**): Representative PET images of nude mice bearing KB tumors at 24 h after intravenous injection of FA-[^{64}Cu]CuS NPs, PEG-[^{64}Cu]CuS NPs, or FA-[^{64}Cu]CuS NPs plus free FA (blocking). Arrows indicate tumors. (**d-f**): Representative autoradiographs of sectioned KB tumor slides at 24 h after radiotracer injection.

Figure 6. *In vitro* assessment of photothermal therapy mediated by FA-CuS NPs. KB cells that overexpress folate receptors were incubated with FA-CuS NPs, PEG-CuS NPs, or FA-CuS NPs plus FA for 2 h and washed. (**a-d**) No laser treatment. (**e-h**) NIR laser irradiation (808 nm, 1.5 W/cm^2 for 2 min). Live cells were stained with calcein AM (green) and dead cells were stained with ethidium homodimer-1 (red).

Figure 7. *In vivo* tumor temperature elevation of tumors in KB tumor-bearing mice with laser irradiation (808 nm at 1.5 W/cm^2, 2 min). Infrared thermal imaging camera was used to measure the temperature change of the tumors under laser irradiation.

Figure 8. CuS NP–induced photothermal destruction of KB tumors *in vivo*. Representative microphotographs of tumors removed 24 h after laser treatment (808 nm at 1.5 W/cm^2, 2 min). The tissues were cryosectioned into 20-μm slices and stained with hematoxylin and eosin. Upper scale bar, 1000 μm; lower scale bar, 50 μm. (**a&d**) FA-CuS NPs plus laser treatment; (**b&e**) PEG-CuS NPs plus laser; (**c&f**) saline plus laser. (**g**) Quantitative analysis of percentage of necrosis induced by various treatments. Necrosis was measured as a percentage of the whole tumor area. Asterisks indicate statistical significance compared to the PEG-CuS NPs and saline control. Error bars, standard deviation (n = 3). *, $p < 0.05$.

Scheme 1

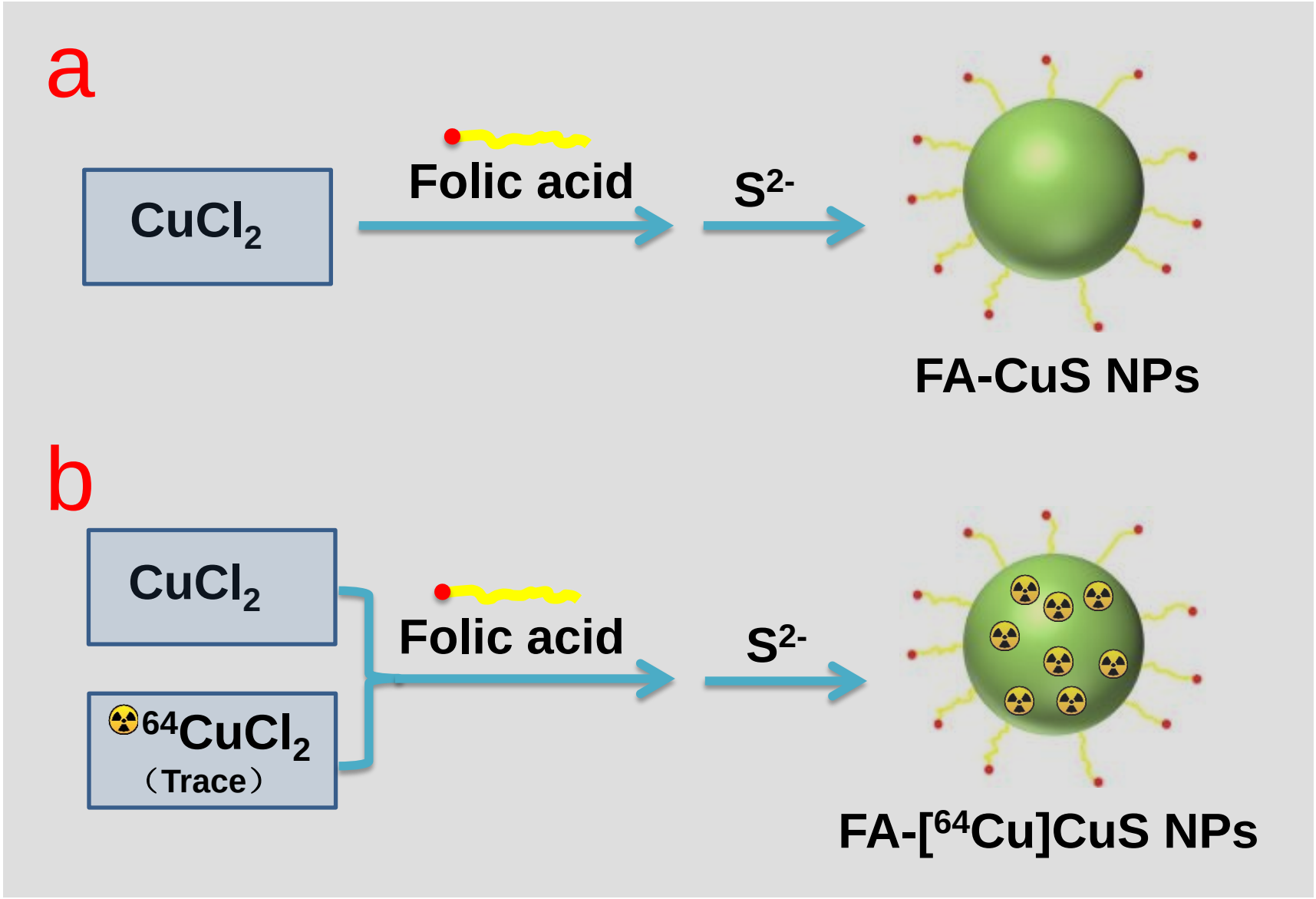

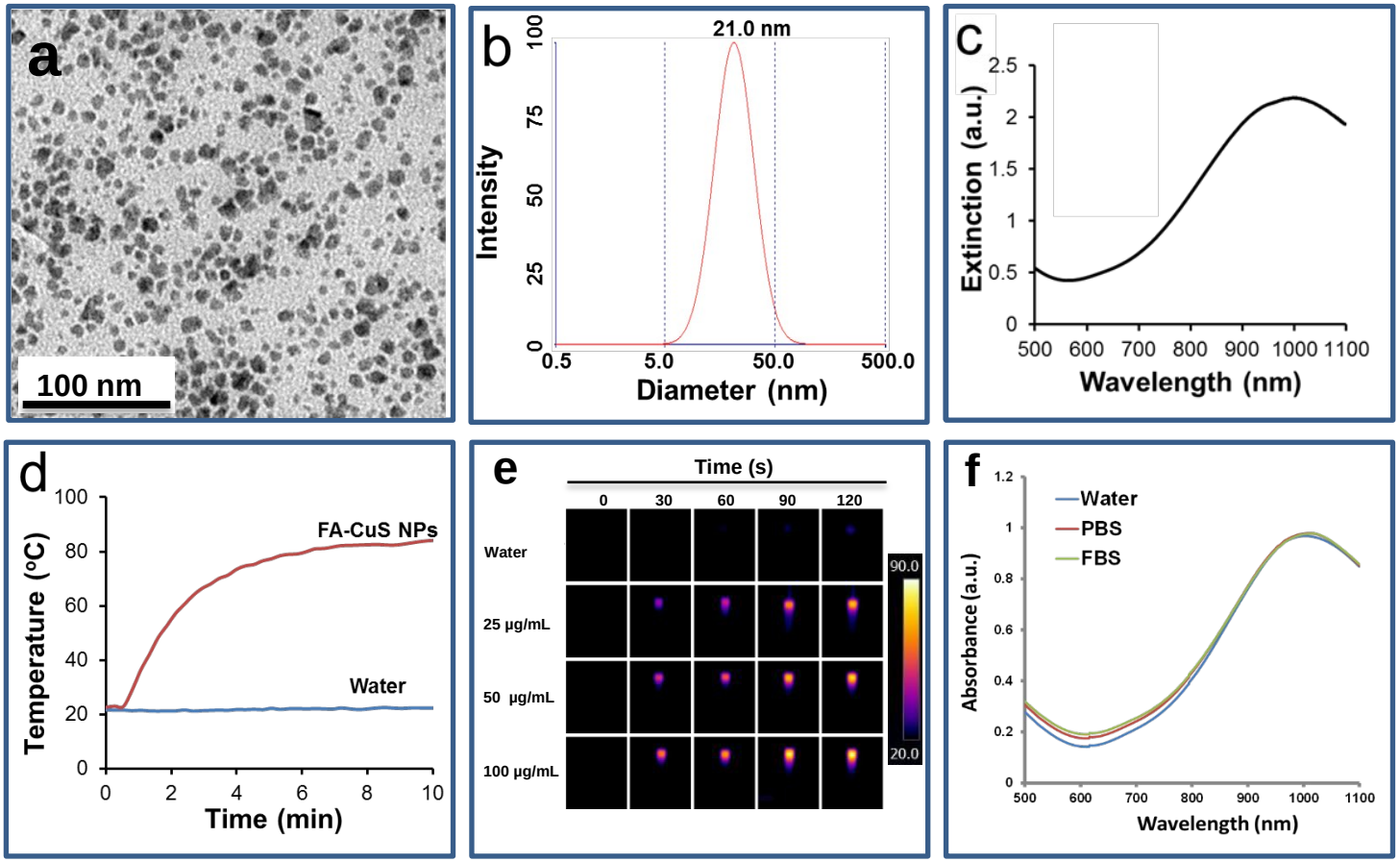

Fig 2.

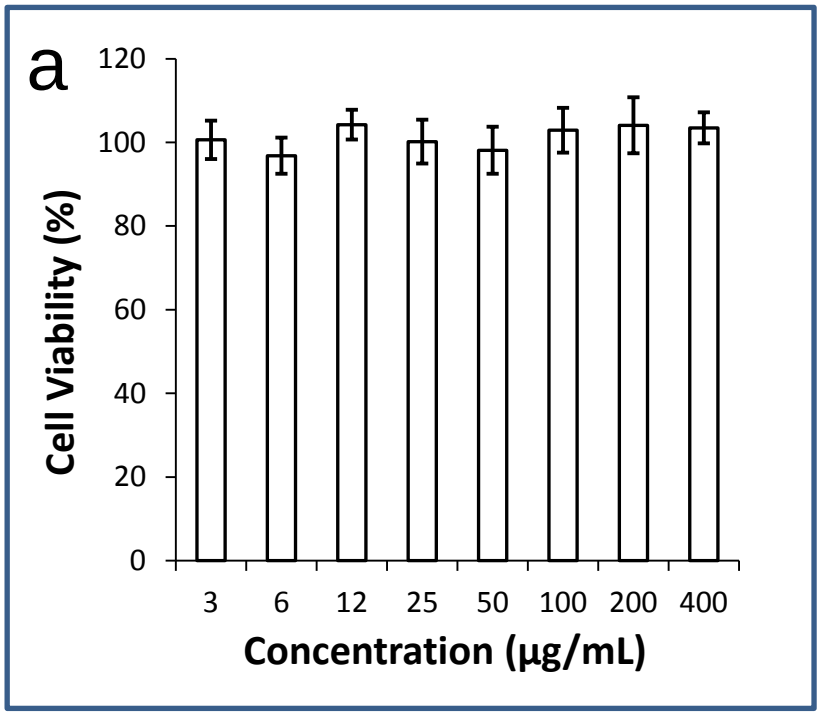

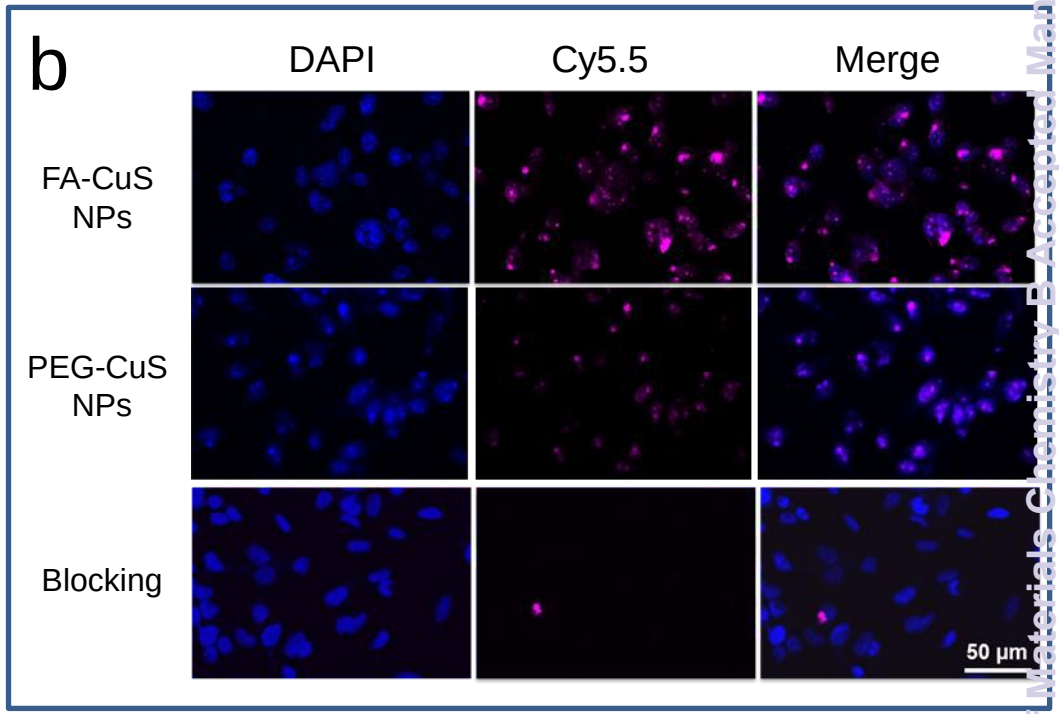

Fig 3.

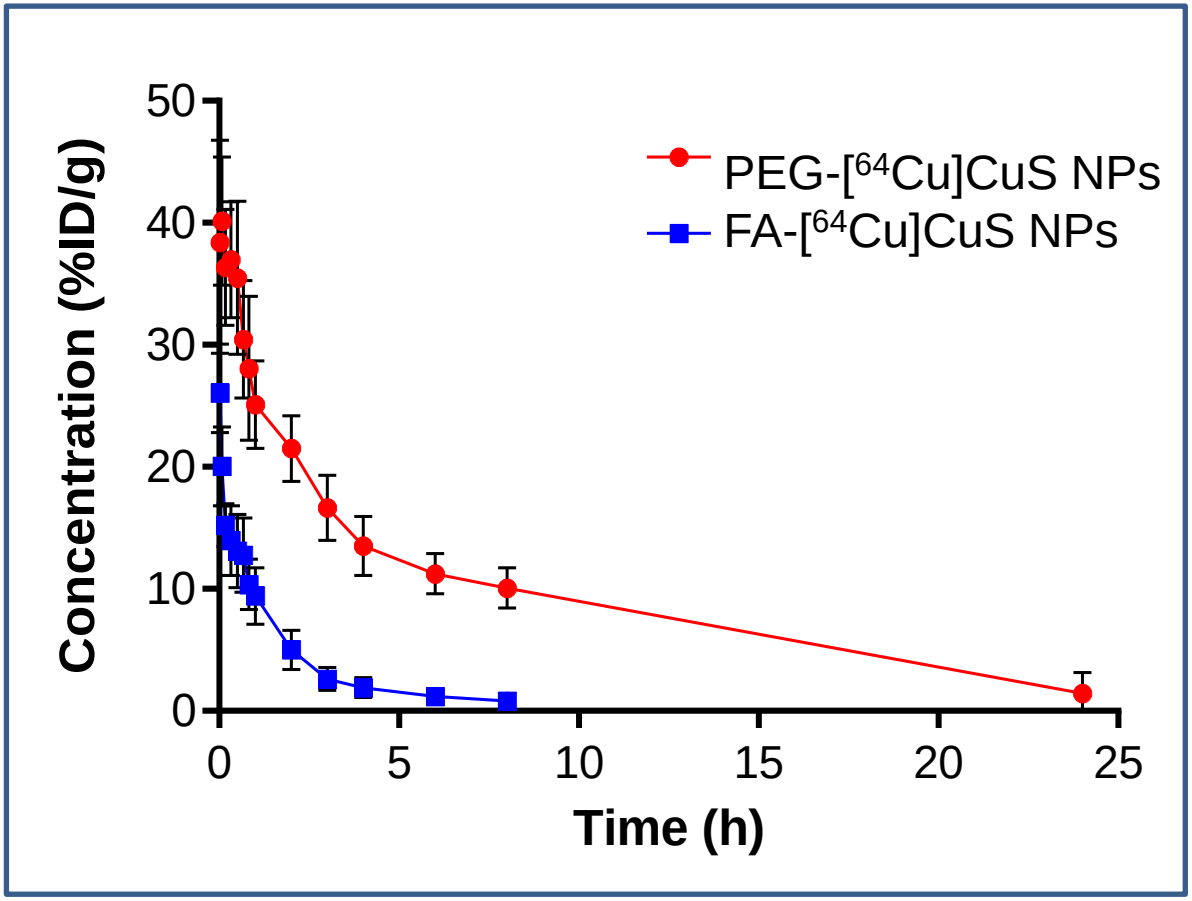

Fig 4.

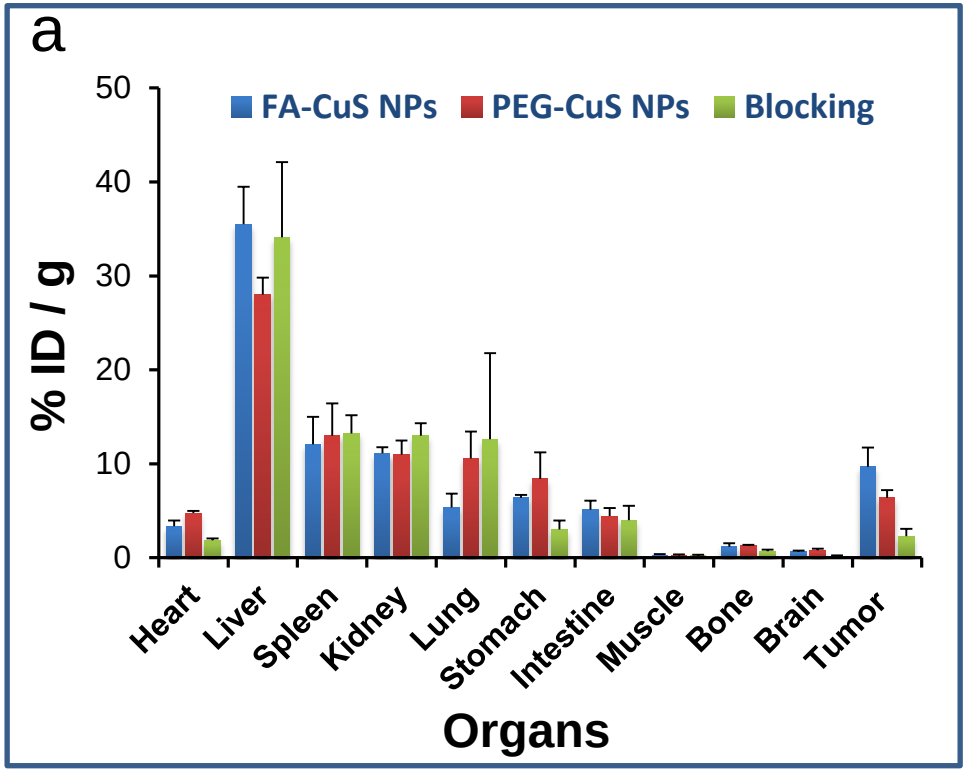

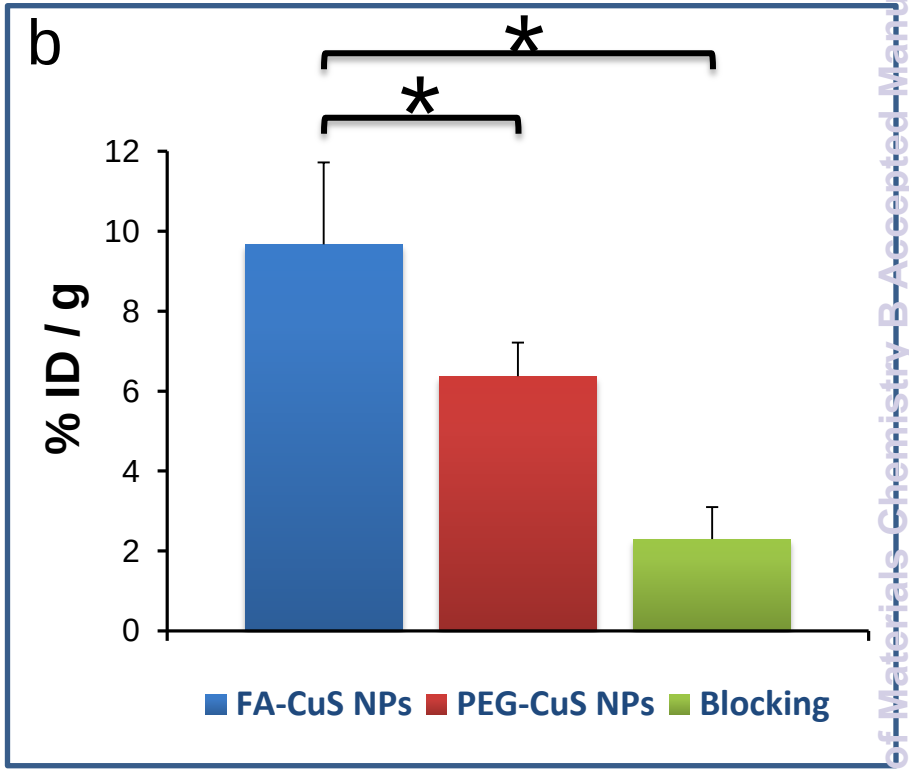

Fig 5.

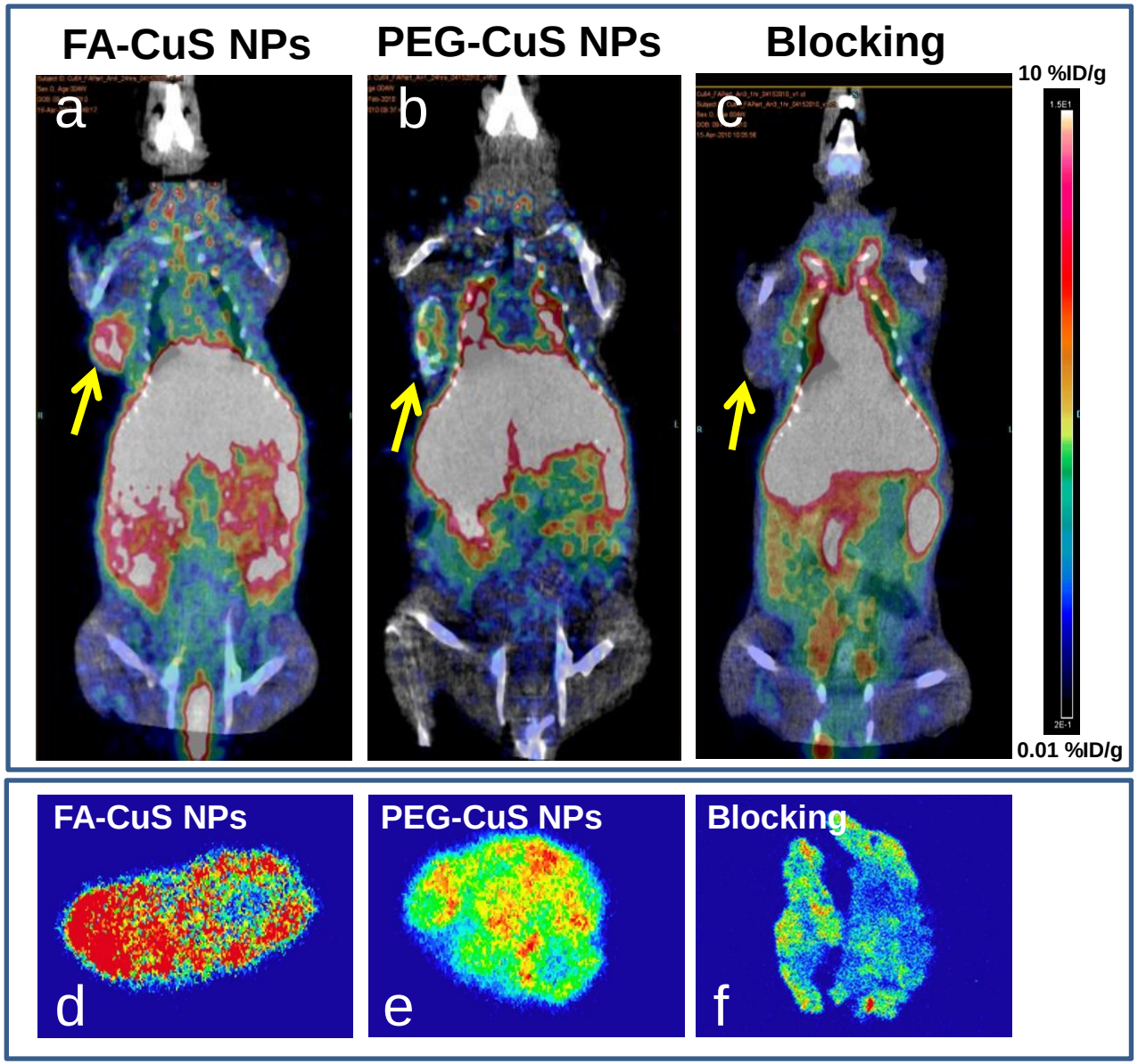

Fig 6.

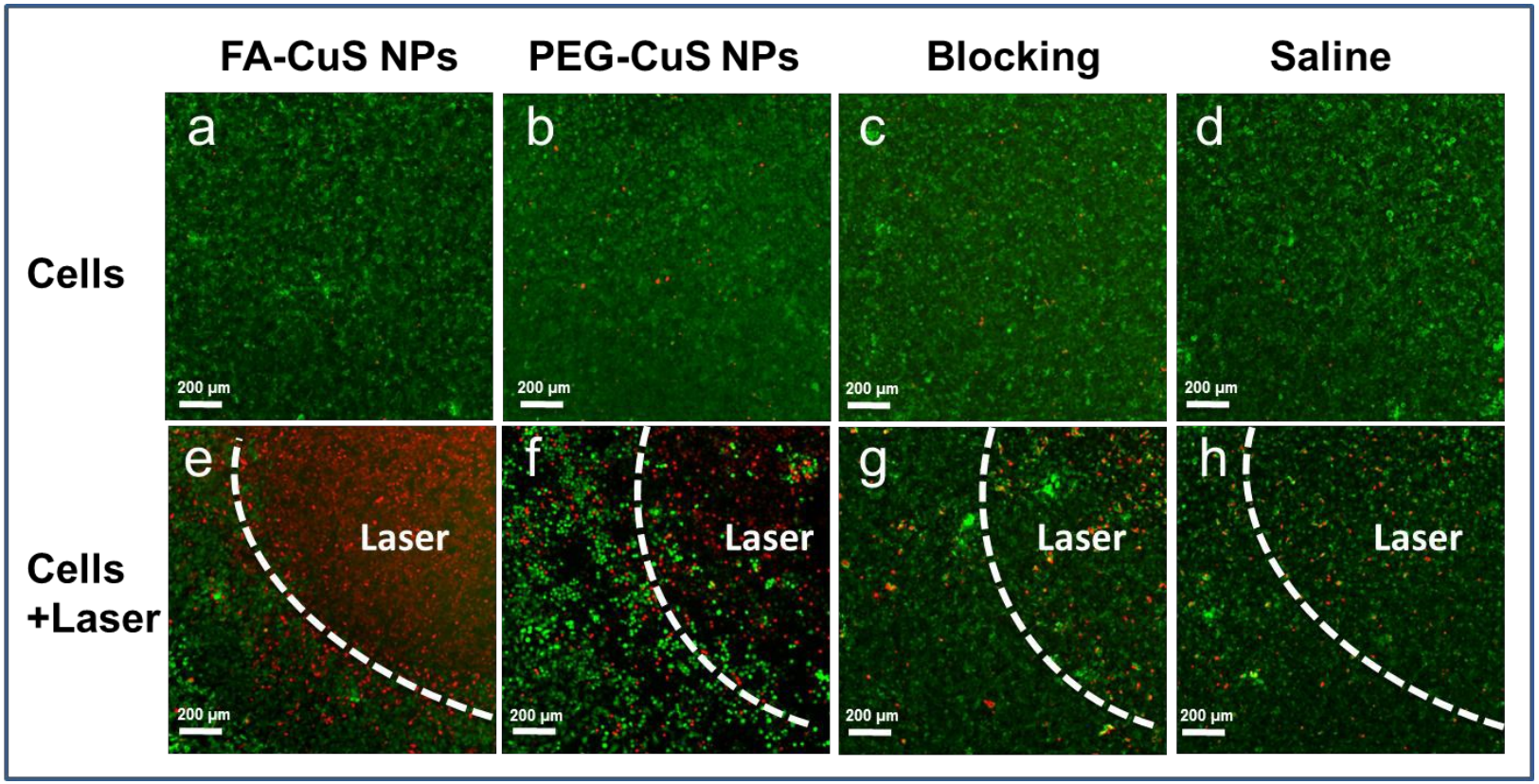

Fig 7.

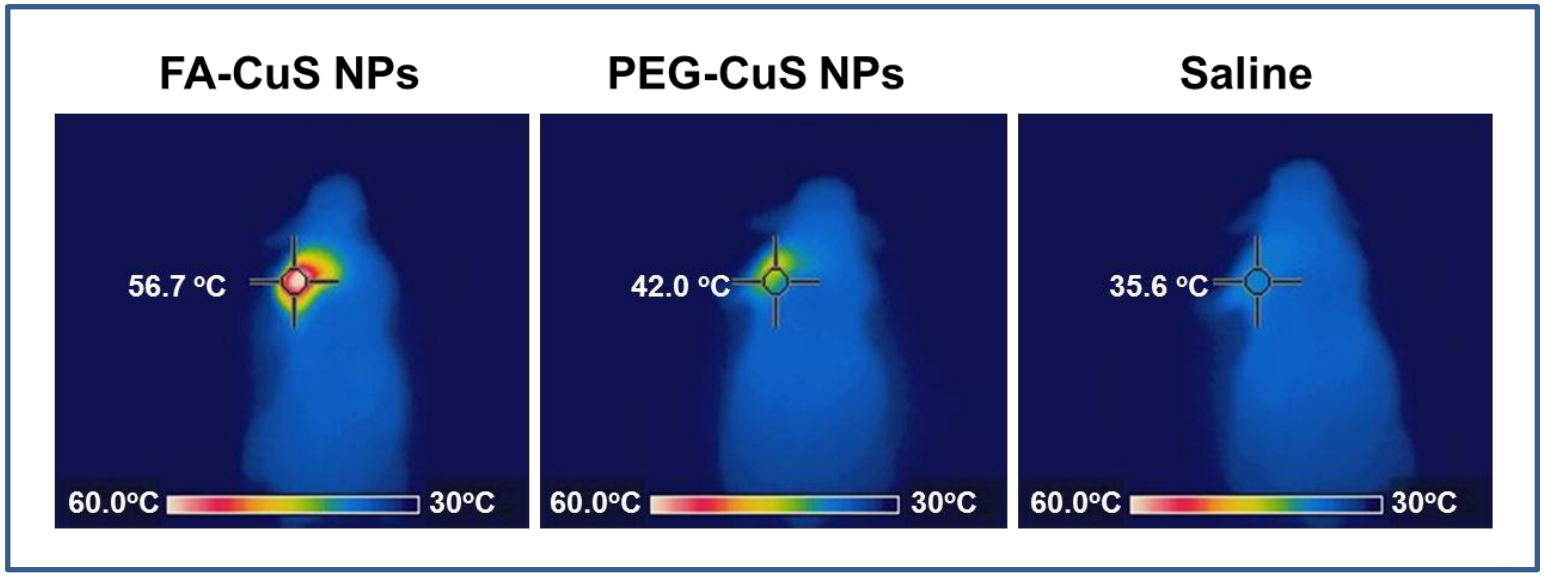

Fig 8.

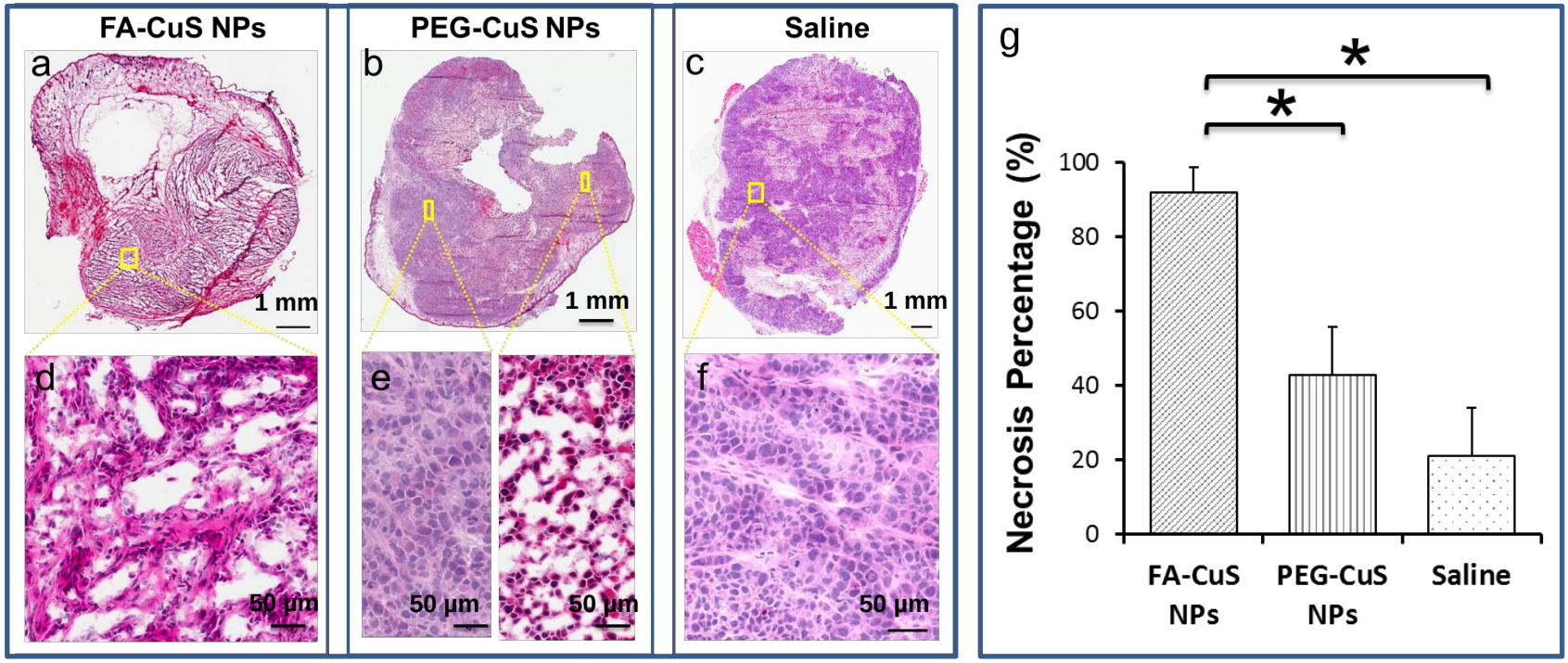

Table of Content

Targeted FA-CuS NPs can significantly improve the tumor uptake; the integration of ^{64}Cu into NPs with strong near-infrared absorption makes them suitable for PET imaging, and image-guided photothermal therapy; targeted FA-CuS NPs mediated substantially greater therapeutic effect compared with photothermal therapy with non-targeted CuS NPs.